NASA Technical Memorandum 85770

NASA-TM-85770 19840013445

TRANSONIC CALCULATION OF AIRFOIL STABILITY AND RESPONSE WITH ACTIVE CONTROLS

J. T. BATINA

T. Y. YANG

MARCH 1984

National Aeronautics and Space Administration

Langley Research Center
Hampton, Virginia 23665

TRANSONIC CALCULATION OF AIRFOIL STABILITY AND RESPONSE WITH ACTIVE CONTROLS

J. T. Batina
NASA Langley Research Center
Hampton, Virginia

T. Y. Yang
Purdue University
West Lafayette, Indiana

Abstract

Transonic aeroelastic stability and response analyses are performed for the MBB A-3 supercritical airfoil. Three degrees of freedom are considered: plunge, pitch, and aileron pitch. The objective of this study is to gain insight into the control of airfoil stability and response in transonic flow. Stability analyses are performed using a Padé aeroelastic model based on the use of the LTRAN2-NLR transonic small-disturbance finite-difference computer code. Response analyses are performed by coupling the structural equations of motion to the unsteady aerodynamic forces of LTRAN2-NLR. The focus of the present effort is on transonic time-marching transient response solutions using modal identification to determine stability. Frequency and damping of these modes are directly compared in the complex s-plane with Padé model eigenvalues. Transonic stability and response characteristics of 2-D airfoils are discussed and comparisons are made. Application of the Padé aeroelastic model and time-marching analyses to flutter suppression using active controls is demonstrated.

Nomenclature

a_h	nondimensional elastic axis location, positive aft of midchord
b	airfoil semi-chord
c_β	nondimensional aileron hinge line location
$[C]$	nondimensional damping matrix
$\{G\}$	control distribution vector
h	plunging d.o.f., positive downward from elastic axis
K_D, K_V, K_A	displacement, velocity, and acceleration control gains, respectively
$[K]$	nondimensional stiffness matrix
m	mass of the airfoil per unit span
M	free stream Mach number
$[M]$	nondimensional mass matrix
p	nondimensional sensor location, positive aft of midchord
$\{p\}$	aerodynamic load vector
r_α, r_β	radii of gyration of airfoil about elastic axis and of aileron about hinge axis, respectively
s	$\sigma+i\omega$, Laplace transform variable
t, $\bar{t}$	time; $\omega_\alpha t$, nondimensional time
U, U^*	free stream velocity; $U/b\omega_\alpha$, nondimensional flight speed
x_α, x_β	nondimensional distances from elastic axis to airfoil mass center and hinge line to aileron mass center, respectively
$\{X\}$, $\{Z\}$	displacement and state vectors, respectively
α	airfoil pitching d.o.f., positive leading edge up
β	aileron pitching d.o.f., positive trailing edge down
β_c	control surface command
ζ_β	control surface viscous damping ratio
μ	$m/\pi\rho b^2$, airfoil mass ratio
ξ	h/b, nondimensional plunging d.o.f., positive downward from elastic axis
ξ_s	nondimensional sensor plunging displacement, positive downward from sensor location
ρ	free stream air density
ω_h, ω_α, ω_β	uncoupled natural frequencies of plunging, pitching about elastic axis, and aileron pitching abut hinge axis, respectively

Introduction

Aeroelastic time-response characteristics of airfoils and wings in transonic flow have recently attracted considerable research interest.[1-6] In the time-response analysis the structural equations of motion are coupled to transonic aerodynamic codes using a numerical integration procedure to calculate transient responses.

Time-marching transient solutions of plunging and pitching airfoils were analyzed by Edwards, et al.,[7] using a complex exponential modal identification technique. Transonic flutter boundaries versus Mach number and angle of attack were determined for the NACA 64A010 and MBB A-3 airfoils. A state-space aeroelastic model employing Padé approximants for the unsteady airloads demonstrated the accuracy of the time-marching technique for the linearized case. Subsequently, Bland and Edwards[8] demonstrated that such locally linear procedures may be used with airloads derived from a transonic small-disturbance code.

Batina[9] studied transonic aeroelastic stability and response behavior of two conventional airfoils, NACA 64A006 and NACA 64A010, and one supercritical airfoil, MBB A-3. In the present study, further results are presented for

the MBB A-3 airfoil. Three degrees of freedom (d.o.f.) are considered: plunge, pitch, and aileron pitch. Response analyses are performed by simultaneously integrating the structural equations of motion along with the unsteady aerodynamic forces of transonic code LTRAN2-NLR.[10] A modal identification technique similar to that of Bennett and Desmarais[11] is applied to the time-marching response curves to identify the aeroelastic modes. Estimated frequency and damping of these modes are plotted in a "root-locus" type format in the complex s-plane. Stability analyses are performed using a state-space aeroelastic model, termed the Padé model, formulated using Padé approximants of the unsteady aerodynamic forces. These forces are described by an interpolating function determined by a least squares curve-fit of LTRAN2-NLR harmonic transonic aerodynamic data. The Padé model is written as a set of linear, first-order, constant coefficient, differential equations. These equations are solved in the Laplace domain yielding eigenvalues compared in the complex s-plane with time-marching modal estimates. The objective of the stability analysis is to investigate the applicability of locally linear aeroelastic modeling to airfoils in transonic flow. Representative Padé model stability results for the NACA 64A010 airfoil were reported in Ref. 12. (The Padé model may alternatively be solved in the time domain with appropriate initial conditions yielding the aeroelastic displacement time-histories.[13])

Open-loop stability and response analyses are performed to determine the behavior of the aeroelastic modes as a function of flight speed. Time-marching response calculations are performed at three different flight speeds to investigate subcritical, critical, and supercritical flutter conditions. Frequency and damping of the aeroelastic modes identified from these transient responses are compared with Padé model results.

Closed-loop stability and response analyses are performed to investigate application of the Padé aeroelastic model and time-marching analyses to flutter suppression using active controls. The control law is intentionally simple for illustrative purposes. Aeroelastic effects due to simple, constant gain, feedback control laws utilizing displacement, velocity, or acceleration sensing are studied using a variety of control gains.

The objective of this study is to gain insight into the control of airfoil stability and response in transonic flow. The focus of the present effort is on time-marching transient response solutions with aeroelastic modal identification. The calculations presented here reveal some interesting aeroelastic behavior discovered when augmenting the aeroelastic system with active controls. Transonic aeroelastic stability and response characteristics of 2-D airfoils are discussed and comparisons are made.

Time-Marching Response Analysis

Response analyses are performed by simultaneously integrating the structural equations of motion along with the unsteady aerodynamic forces of the transonic code LTRAN2-NLR. The equations of motion for a typical airfoil section oscillating with three d.o.f.'s can be written as[9,12-14]

$$[M]\{\ddot{X}\} + [C]\{\dot{X}\} + [K]\{X\} = \{p\} + \{G\}\beta_c \qquad (1)$$

where $\{X\} = [\xi \ \alpha \ \beta]^T$ is the displacement vector containing plunge displacement ξ, pitching rotation α, and aileron pitching rotation β. The dot denotes differentiation with respect to nondimensional time $\omega_\alpha t$.

For closed-loop study, a simple, constant gain, feedback control law has been assumed of the form

$$\beta_c = K_D\xi_s + K_V\dot{\xi}_s + K_A\ddot{\xi}_s \qquad (2)$$

where K_D, K_V, and K_A are the displacement, velocity, and acceleration control gains, respectively; ξ_s is the sensor measured plunging motion. A single sensor was placed along the airfoil chord to obtain a measure of airfoil plunge and pitch motions from

$$\xi_s = \lfloor H \rfloor \{X\} \qquad (3)$$

where $\lfloor H \rfloor = \lfloor 1 \ (p-a_h) \ 0 \rfloor$ and p is the sensor location aft of midchord.

The control system consists of a single sensor located near the control surface hinge line at 70% chord (p = 0.4), the control law, Eq. (2), and a trailing edge control surface of 25% chord. With this system, control surface aerodynamic forces are utilized to alleviate flutter instability. Details of the control system and equations may be found in Ref. 12.

By expressing the control law Eq. (2) in terms of the airfoil motion, the aeroelastic equations of motion may be written in general form for time-integration as

$$[M^*]\{\ddot{X}\} + [C^*]\{\dot{X}\} + [K^*]\{X\} = \{p\} \qquad (4)$$

where $[M^*] = [M] - K_A\{G\}\lfloor H \rfloor$ (5a)

$$[C^*] = [C] - K_V\{G\}\lfloor H \rfloor \qquad (5b)$$

$$[K^*] = [K] - K_D\{G\}\lfloor H \rfloor \qquad (5c)$$

Details of the time-marching response solution procedures were given in Ref. 13.

A modal identification technique is used to determine the damping, frequency, amplitude, and phase of the aeroelastic modes from the time-marching displacement response histories. A method similar to that of Bennett and Desmarais[11] was used to least-squares curve-fit the time responses by complex exponential functions in the form

$$x(\bar{t}) = a_0 + \sum_{j=1}^{m} e^{\left(\frac{\sigma}{\omega_\alpha}\right)_j \bar{t}} \left[a_j \cos \left(\frac{\omega}{\omega_\alpha}\right)_j \bar{t} + b_j \sin \left(\frac{\omega}{\omega_\alpha}\right)_j \bar{t}\right] \qquad (6)$$

The damping and frequency of the complex modes thus obtained

$$\left(\frac{\sigma}{\omega_\alpha}\right)_j + i\left(\frac{\omega}{\omega_\alpha}\right)_j = \left(\frac{s}{\omega_\alpha}\right)_j \qquad (7)$$

are estimates of the aeroelastic eigenvalues and may then be directly compared in the complex s-plane with those computed by the Padé model.

As an example, Fig. 1 shows a typical response analysis of the MBB A-3 airfoil at $M = 0.765$ and $c_\ell = 0.58$. The LTRAN2-NLR time-marching pitching response α and the modal curve fit using Eq. (6) are shown in the top part of the figure. Only the data used for curve fitting (144 points) is shown. In the lower part of the figure are the two component aeroelastic modes, identified from the modal fit.

Padé Model Stability Analysis

Stability analyses are performed using a linear eigenvalue analysis of the Padé model. This model was formulated by curve-fitting the unsteady aerodynamic forces by a Padé approximating function.[9,12] These approximating functions are then expressed as linear differential equations which, when coupled to the structural equations of motion, lead to the first-order matrix equation

$$\{\dot{Z}\} = \frac{s}{\omega_\alpha}\{Z\} = [A]\{Z\} + \{B\}\beta_c \qquad (8)$$

where $\{Z\}$ is the state vector containing displacement, velocity, and augmented states; s/ω_α is the complex eigenvalue. By expressing the control law Eq. (2) in terms of the state-vector $\{Z\}$, Eq. (8) is easily solved using standard eigenvalue solution techniques. Details of the Padé model formulation are given in Ref. 12.

Results and Discussion

Transonic aeroelastic stability and response analyses were reported in Ref. 9 for three airfoil configurations: NACA 64A006, NACA 64A010, and MBB A-3. All three airfoils are among those proposed by AGARD for aeroelastic applications of transonic unsteady aerodynamics.[15] Aeroelastic behavior of the MBB A-3 airfoil was studied at the design Mach number $M = 0.765$ and at (1) zero mean angle of attack $\alpha = 0^0$; and (2) the design steady lift coefficient $c_\ell = 0.58$. The mean angle of attack necessary to match $c_\ell = 0.58$ using LTRAN2-NLR is $\alpha = 0.86^0$. In this report, representative time-marching response histories and s-plane stability root-loci for the MBB A-3 airfoil at $M = 0.765$ and $c_\ell = 0.58$ are presented. Aeroelastic parameter values selected are the same as those used in Refs. 12 and 13 and are listed in Table 1.

Table 1. Aeroelastic parameter values for stability and response analyses.

$\omega_h/\omega_\alpha = 0.3$	$x_\alpha = 0.2$
$\omega_\beta/\omega_\alpha = 1.5$	$r_\alpha = 0.5$
$\mu = 50.0$	$x_\beta = 0.008$
$a_h = -0.2$	$r_\beta = 0.06$
$c_\beta = 0.5$	$\zeta_\beta = 0.0$

Steady pressure solutions are required as aerodynamic initial conditions for unsteady calculations. As an example, the MBB A-3 steady pressure distribution computed using LTRAN2-NLR at $M = 0.765$ and $c_\ell = 0.58$ is shown in Fig. 2 along with the airfoil contour. This steady pressure data compares well with the experimental results of Bucciantini et al.[16] There is a relatively weak shock wave on the airfoil upper surface near 55% to 60% chord. Steady pressure distributions for all of the cases considered indicate shock locations in the range of 50% to 65% chord and shock strengths that are well within the range of applicability of transonic small-disturbance theory.[9]

Open-Loop

Open-loop stability and response analyses are performed to determine the behavior of the aeroelastic modes as a function of flight speed. These calculations were first performed using the Padé aeroelastic model with results plotted in a flight speed root-locus format. As an example, open-loop root-loci as a function of flight speed are presented in Fig. 3 for the MBB A-3 airfoil. With increasing flight speed, the torsion branch moves to the left in the stable left-half of the complex s-plane. The aileron branch is also stable throughout, moving up and to the left as flight speed is increased. The bending dominated root-locus becomes the flutter mode at a nondimensional flutter speed of $U_F^* = 2.370$. In addition, the Padé model also predicts the divergence speed, where an aerodynamic lag root moves onto the positive real axis, as $U_D^* = 3.320$. This divergence phenomenon is similar to that reported by Edwards,[14] where static divergence of a typical section in incompressible flow occurred due to the emergence of a real positive root from the complex s-plane origin. In Ref. 14, this root appeared in addition to the original structural poles and was also predicted using a Padé model. Table 2 compares the flutter and divergence speeds with those computed using linear aerodynamic theory. Flutter speeds from a p-k method flutter analysis are also tabulated for further comparison. These p-k method calculations were performed to assess the accuracy of the Padé model flutter solution. Padé model flutter speeds compare well with the p-k method values.

Table 2. Summary of open-loop flutter and divergence speeds for the MBB A-3 airfoil at M = 0.765.

AIRFOIL	FLUTTER METHOD	FLUTTER SPEED U_F^*	DIVERGENCE SPEED U_D^*	$\frac{U_D}{U_F}$
MBB A-3 c_ℓ =0.58	Padé	2.370	3.320	1.401
	p-k	2.403		
LINEAR THEORY	Padé	2.711	3.611	1.332
	p-k	2.729		

Time-marching transient responses were then obtained at three different flight speeds to investigate subcritical, critical, and supercritical flutter conditions. These calculations were performed independent of the Padé approximation, primarily for verification purposes. Transient response histories are shown in Fig. 4 for three values of flight speed near the flutter speed. A one-percent semi-chord plunge displacement was used as initial condition. Time-responses for U/U_F = 1.0 in Fig. 4 are nearly neutrally stable corresponding to the flutter condition. The flutter speed used for time-marching analyses was the p-k method value. Aeroelastic transients for U/U_F = 0.844 and U/U_F = 1.156 in Fig. 4 show converging (subcritical) and diverging (supercritical) oscillatory behavior, respectively.

Damping and frequency estimates of the aeroelastic modes were determined from the time-response histories of Fig. 4. These estimates are compared with Padé model eigenvalues for the bending and torsion modes in Fig. 5. In general, the Padé results compare well with the time-marching modal frequency and damping values. Agreement for the lower frequency bending mode is, in general, better than that for the higher frequency torsion mode. Frequency and damping estimates for the aileron mode are much less accurate than those for bending and torsion. The above discrepancies are attributed to: (1) the Padé model is less accurate at the higher damping ratios involved; (2) the structural integration is performed with fewer time-steps per cycle of the higher frequency modes; and (3) since the aileron mode has much more damping in comparison with bending and torsion, its contribution to the responses dies out quickly leaving very little information for modal curve-fitting.

Closed-Loop

The Padé aeroelastic model was used to study the effects of active feedback control on the aeroelastic modes at the flight speed equal to the open-loop flutter value. These calculations were performed primarily to determine the range and sign of the control gains required to stabilize the flutter mode. Padé stability calculations were also performed at the same Mach numbers using linear subsonic aerodynamic theory for comparison with transonic Padé model results. Effects due to displacement, velocity, and acceleration feedback were further assessed using time-marching response analyses for comparison with Padé results. Finally, an example is presented illustrating the effectiveness of velocity feedback upon flutter suppression at speeds above and below the open-loop flutter speed.

Effects of Active Control on Flutter Mode.- Closed-loop analyses are first performed at the flight speed equal to the open-loop flutter value, to determine the behavior of the aeroelastic modes as a function of control gain. Effects of active control on the bending dominated flutter mode are of primary interest. Control gain root-loci computed using the Padé model for displacement, velocity, and acceleration control laws are shown in the left, center, and right of Fig. 6, respectively. Corresponding root-loci computed using linear subsonic theory are given in Fig. 7. In each case there are three open-loop aeroelastic roots or "poles" corresponding to the three structural d.o.f.'s. The two poles in the stable left-half of the complex s-plane correspond to the torsion and aileron modes; the pole that lies on the imaginary axis is the bending dominated flutter mode. These aeroelastic roots move toward "zeros" of the aeroelastic transfer function as the control gains K_D, K_V, or K_A are monotonically increased or decreased. Solid-line root-loci indicate the sign of the control gain that stabilizes the flutter mode whereas the dashed-line loci indicate the opposite effect. Comparison of LTRAN2-NLR results of Fig. 6 with the linear theory results of Fig. 7 indicates that frequency and damping values are significantly different for transonic and subsonic cases, although the overall root-locus trends are similar. This lack of agreement between linear theory results and LTRAN2-NLR root-loci illustrates the importance of including transonic effects in aeroelastic stability calculations.

Displacement feedback with negative control gains easily stabilized the flutter mode as shown in Figs. 6 and 7. Negative displacement feedback, however, results in static divergence of the same nature found in the open-loop cases. For the MBB A-3 airfoil at M = 0.765 and c_ℓ = 0.58, this occurs for $K_D \leq -0.5$. Divergence root locations are shown in Figs. 6 and 7 for K_D = -1.0. Also, positive displacement feedback destabilized the flutter mode.

Velocity feedback with positive control gains stabilized the bending dominated flutter pole and increased the damping of the torsion mode. The transonic results of Fig. 6 indicate that there is more damping in bending and aileron modes, and much less in torsion than predicted by linear subsonic theory in Fig. 7. Also, negative velocity feedback destabilized the flutter mode.

Acceleration feedback with positive control gains stabilized the flutter pole and decreased damping and frequency of the torsion mode. Also, negative acceleration feedback destabilized the flutter mode.

Effects Due to Displacement Feedback. - Aeroelastic effects due to displacement feedback, ξ_s, were further studied by obtaining time-marching transient responses for $K_D = -1.0$ and detailed Padé stability results for the range of displacement gains $-1.0 \leq K_D \leq 0.0$. These calculations were performed primarily to investigate the divergence phenomenon predicted by a positive real aerodynamic lag root in the Padé model. The three d.o.f. time-histories computed using LTRAN2-NLR at $U/U_F = 1.0$ and $K_D = -1.0$ are given in Fig. 8. These responses show that flutter has been suppressed and that the aeroelastic displacements are indeed divergent. Comparisons of time-marching frequency and damping estimates with Padé eigenvalues are shown in Fig. 9. Good agreement is found in predicting this aeroelastic divergence. In addition, negative displacement feedback increased the damping in bending and decreased the torsion mode frequency. The lower frequency bending mode damping and frequency values for $K_D = -1.0$ compare well; results from the time-marching modal fits for the higher frequency torsion and aileron modes were not reliably determined.

Padé stability calculations were then performed for the range of gains $-1.0 \leq K_D \leq 0.0$ to reveal the effects of negative displacement feedback on flutter and divergence speeds. These more detailed results are shown in Fig. 10 for the MBB A-3 airfoil. Negative displacement feedback slowly increases the flutter speed and first rapidly increases the divergence speed. For gains K_D between approximately -0.2 and -0.5, divergence is eliminated. In this region, the aerodynamic lag root previously causing divergence no longer crosses through the origin. For $K_D \leq -0.5$, divergence reappears as the critical mode of instability at speeds much lower than flutter. The flutter speed is increased approximately 14% for $K_D \approx -0.5$.

Effects Due to Velocity Feedback. - Aeroelastic effects due to velocity feedback, $\dot{\xi}_s$, were further investigated by obtaining transient responses for successively increased velocity feedback. These calculations are first performed at the flight speed $U^* = U_F^*$. Values selected for the control gains were $K_V = 3.0$, 6.0, and 9.0, the same gains shown by the triangles in the center portion of Fig. 6. LTRAN2-NLR response results are shown in Fig. 11. These response histories show that as K_V is increased the dominant motion is consistently more damped and of higher frequency. Also, positive velocity feedback significantly increased the nonrational part[14] of the plunge displacement responses. Here, the ξ-transients oscillate about an asymptotically decaying rather than a zero mean value.

Damping and frequency of the aeroelastic modes determined from the LTRAN2-NLR displacement transients are plotted in Fig. 12 along with Padé model results. The flutter mode damping and frequency are both successively increased for values of $K_V = 3.0$, 6.0, and 9.0. The torsion mode damping is significantly increased with little effect upon the torsion mode frequency. Comparison of Padé eigenvalues with time-marching modal estimates shows general agreement. Discrepancies between the two sets of results are attributed to the same reasons as in the open-loop case. Also, the torsion mode for $K_V = 6.0$ and 9.0 could not be identified from the time-marching transients because of the large increase in damping.

Velocity feedback with positive control gains suppressed flutter for the range of flight speeds investigated. Some sensitivity with respect to mean angle of attack has been observed though in calculations using velocity feedback.[12] For the MBB A-3 airfoil at $M = 0.765$ and zero mean angle of attack, the flutter speed was increased by only 11% for the gain $K_V = 9.0$. Additional calculations also showed that velocity feedback does not affect the divergence speed. Therefore for the $c_\ell = 0.58$ case, the aeroelastic instability becomes that of static divergence. Since the control law with velocity feedback was found to be generally the most effective in raising flutter speeds,[12] more detailed calculations were performed. These results are described in a following section entitled "Illustrative Example."

Effects Due to Acceleration Feedback. - Aeroelastic effects due to acceleration feedback, $\ddot{\xi}_s$, were further investigated by obtaining transient responses for successively increased acceleration feedback. These calculations are performed at the flight speed $U^* = U_F^*$. Values selected for the control gains were $K_A = 6.0$, 12.0, and 18.0, the same gains shown by the triangles in the right portion of Fig. 6. LTRAN2-NLR response results are shown in Fig. 13. These response histories show that as K_A is increased the dominant motion is consistently more damped and of lower frequency. Also, a higher frequency transient becomes more visible in the α and β responses for the larger values of K_A. This is due to the decreased damping of the torsion mode as shown in the frequency and damping comparisons of Fig. 14. Positive acceleration feedback increased damping in bending, decreased damping in torsion, and lowered the frequencies of both modes. Comparison of Padé eigenvalues with time-marching modal estimates shows general agreement. Results for the lower frequency bending mode are in better agreement than results for the higher frequency torsion mode.

Acceleration feedback with positive control gains raised the flutter speed approximately 25% for the maximum gain studied, $K_A = 18.0$. Additional calculations showed that acceleration feedback does not affect the divergence speed.

Illustrative Example. - Additional aeroelastic analyses were performed at speeds above and below the open-loop flutter speed using the velocity feedback control law since this control law was found to be generally the most effective.[12] These results are presented to further illustrate application of the Padé

and time-marching methods. Padé flight speed root-loci are shown in Fig. 15 for values of the velocity gain K_V = 3.0, 6.0, and 9.0. Positive velocity feedback significantly increased the damping of the torsion root-locus and decreased the damping of the aileron mode. The bending root-locus for K_V = 3.0 reflects an increase in flutter speed of approximately 29% (U_F^* = 3.050), while for K_V = 6.0 and 9.0 flutter has been eliminated. Since velocity feedback does not affect the divergence speed, the aeroelastic instability becomes that of static divergence at the uncontrolled divergence speed U_D^* = 3.320. This divergence speed is approximately 40% greater than the open-loop flutter speed as shown in Table 2.

Time marching response calculations were then performed for U/U_F = 1.266 using LTRAN2-NLR to complement and verify the Padé model results. These response histories shown in Fig. 16, correspond to the U^* = 3.0 diamond-symbol eigensolutions of Fig. 15. These aeroelastic transients are bending dominated and converging for all three values of the control gain K_V. As K_V is increased, the responses become more stable indicating a monotonic increase in bending mode damping, at approximately the same frequency. Again, positive velocity feedback significantly increased the nonrational part of the plunge displacement responses.

Effects of velocity feedback on bending and torsion modes at U/U_F = 1.266 are shown in Fig. 17. Because of the large damping increase in torsion due to K_V and the relatively high frequency of the aileron mode, only the bending mode was determined from the aeroelastic transients of Fig. 16. Comparison of the two sets of bending root-locus results in Fig. 17 shows very good agreement. Positive velocity feedback increased bending mode damping at approximately the same frequency.

Finally, open and closed-loop flight speed root-loci are shown in Fig. 18 for both bending and torsion modes. The velocity feedback gain used to generate the closed-loop results is K_V = 9.0, the same value used in the right portion of Fig. 15. Padé model and time-marching solutions for the bending mode compare well. The control gain K_V = 9.0 increased the torsion mode damping for the range of flight speeds $0.844 \leq U/U_F \leq 1.266$, such that the results do not permit comparison between Padé and time-marching solutions. Fig. 18 illustrates again that positive velocity feedback has eliminated the flutter instability for the MBB A-3 airfoil at M = 0.765 and c_ℓ = 0.58.

Conclusions

Transonic aeroelastic stability and response calculations have been performed for 2-D airfoils using the LTRAN2-NLR transonic small-disturbance code. Representative results are presented here for the MBB A-3 airfoil at the design condition M = 0.765 and c_ℓ = 0.58. Emphasis is placed on time-marching transient response solutions with modal identification for comparison with Padé model eigenvalues. Extension of the time-marching transient response analysis to a three degree of freedom aeroelastic system including active controls is demonstrated. Accurate frequency and damping estimates were obtained using a complex exponential least squares curve-fit of the aeroelastic responses. Good agreement was found between s-plane eigenvalues calculated using the Padé aeroelastic model and time-marching modal estimates. Therefore, locally linear aeroelastic modeling was found to be applicable to 2-D airfoils in small-disturbance transonic flow, for cases that are within the range of validity of the transonic codes. The importance of including transonic effects in aeroelastic stability calculations was illustrated by the differences between root-loci calculated using linear subsonic theory and LTRAN2-NLR. Although the overall root-locus trends are similar, frequency and damping values are significantly different for transonic and subsonic cases.

Effects due to simple, constant gain, control laws utilizing displacement, velocity, or acceleration sensing were studied. Displacement feedback with negative control gains suppressed flutter but caused airfoil responses to diverge. Comparison of Padé eigenvalues with time-marching frequency and damping estimates showed good agreement in predicting this aeroelastic divergence. In addition, negative displacement feedback increased the damping in bending, and decreased the torsion mode frequency. Detailed Padé stability calculations revealed the effects of negative displacement feedback on flutter and divergence speeds. Velocity feedback with positive control gains suppressed flutter. Padé stability results compared well with time-marching frequency and damping values. In general, positive velocity feedback increased damping in both bending and torsion modes, and significantly increased the nonrational part of the plunge displacement responses. Here, the plunge transients oscillated about an asymptotically decaying rather than a zero mean value. Acceleration feedback with positive control gains also increased flutter speeds. Again, Padé results compared well with time-marching modal estimates. In general, positive acceleration feedback increased damping in bending, decreased damping in torsion, and lowered the frequencies of both modes.

References

[1]Ballhaus, W. F. and Goorjian, P. M., "Computation of Unsteady Transonic Flows by the Indicial Method," AIAA Journal, Vol. 16, Feb. 1978, pp. 117-124.

[2]Rizzetta, D. P., "Time-Dependent Responses of a Two-Dimensional Airfoil In Transonic Flow," AIAA Journal, Vol. 17, Jan. 1979, pp. 26-32.

[3]Guruswamy, P. and Yang, T. Y., "Aeroelastic Time Response Analysis of Thin Airfoil by Transonic Code LTRAN2," Journal of Computers and Fluids, Vol. 9, Dec, 1981, pp. 409-425, (Also AFFDL-TR-79-3077, June 1979).

[4]Borland, C. J. and Rizzetta, D. P., "Nonlinear Transonic Flutter Analysis," AIAA Journal, Vol. 20, Nov. 1982, pp. 1606-1615.

[5]Yang, T. Y. and Chen, C. H., "Transonic Flutter and Response Analyses of Two Three-Degree-of-Freedom Airfoils," Journal of Aircraft, Vol 19, Oct 1982, pp. 875-884, (Also AFWAL-TR-81-3103, Aug. 1981).

[6]Yang, T. Y. and Batina, J. T., "Transonic Time-Response Analysis of Three D.O.F. Conventional and Supercritical Airfoils," Journal of Aircraft, Vol. 20, Aug. 1983, pp. 703-710.

[7]Edwards, J. W., Bennett, R. M., Whitlow, W., Jr. and Seidel, D. A., "Time-Marching Transonic Flutter Solutions Including Angle-of-Attack Effects, Journal of Aircraft, Vol. 20, Nov. 1983, pp. 899-906.

[8]Bland, S. R. and Edwards, J. W., "Airfoil Shape and Thickness Effects on Transonic Airloads and Flutter," AIAA Paper No. 83-0959, presented at the AIAA/ASME/ASCE/AHS 24th Structures, Structural Dynamics and Materials Conference, Lake Tahoe, NV, May 2-4, 1983, also Journal of Aircraft, Vol. 21, March 1984, pp. 209-217.

[9]Batina, J. T., "Transonic Aeroelastic Stability and Response of Conventional and Supercritical Airfoils Including Active Controls," Ph.D. Thesis, Purdue University, West Lafayette, December 1983.

[10]Houwink, R. and van der Vooren, J., "Results of an Improved Version of LTRAN2 for Computing Unsteady Airloads on Airfoils Oscillating in Transonic Flow," AIAA Paper 79-1553, AIAA 12th Fluid and Plasma Dynamics Conference, Williamsburg, VA., July 23-25, 1979.

[11]Bennett, R. M. and Desmarais, R. N., "Curve Fitting of Aeroelastic Transient Response Data with Exponential Functions in Flutter Testing Techniques," NASA SP-415, 1975, pp. 43-58.

[12]Batina, J. T. and Yang, T. Y., "Application of Transonic Codes to Aeroelastic Modeling of Airfoils Including Active Controls," accepted for publication in Journal of Aircraft.

[13]Batina, J. T. and Yang, T. Y., "Transonic Time-Responses of the MBB A-3 Supercritical Airfoil Including Active Controls," submitted for review to Journal of Aircraft.

[14]Edwards, J. W., "Unsteady Aerodynamic Modeling and Active Aeroelastic Control," SUDAAR 504, Stanford University, Feb. 1977.

[15]Bland, S. R., "AGARD Two-Dimensional Aeroelastic Configurations," AGARD-AR-156, August 1979.

[16]Bucciantini, G., Oggiano, M. S., and Onorato, M., "Supercritical Airfoil MBB A-3, Surface Pressure Distributions, Wake and Condition Measurements," AGARD-AR-138, May 1979, pp. A8-1 to A8-25.

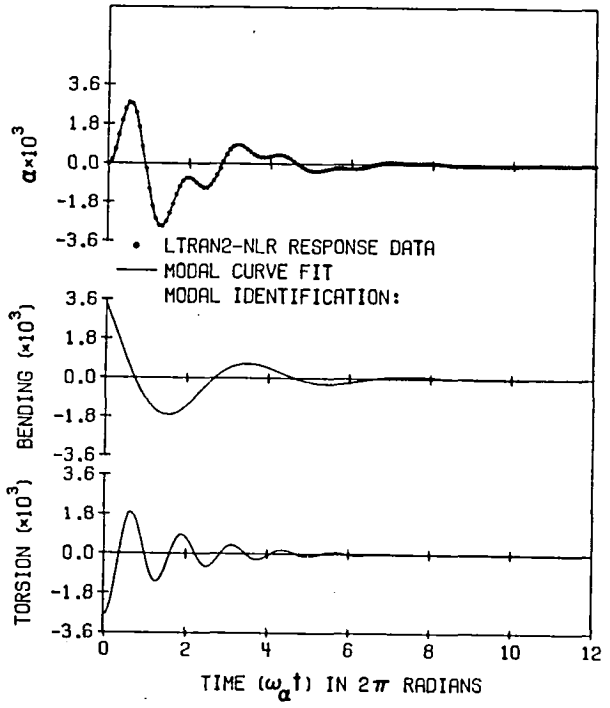

Fig. 1 Modal curve fit of aeroelastic time-marching pitching response of the MBB A-3 airfoil at the open-loop flutter speed $U/U_F = 1.0$, $K_A = 18.0$, $M = 0.765$, and $c_\ell = 0.58$.

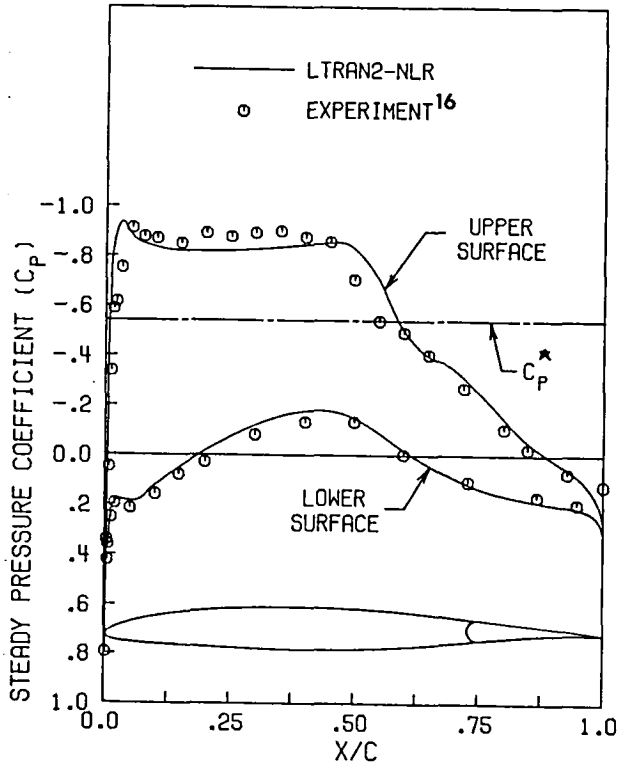

Fig. 2 Steady pressure distributions for the MBB A-3 airfoil at $M = 0.765$ and $c_\ell = 0.58$.

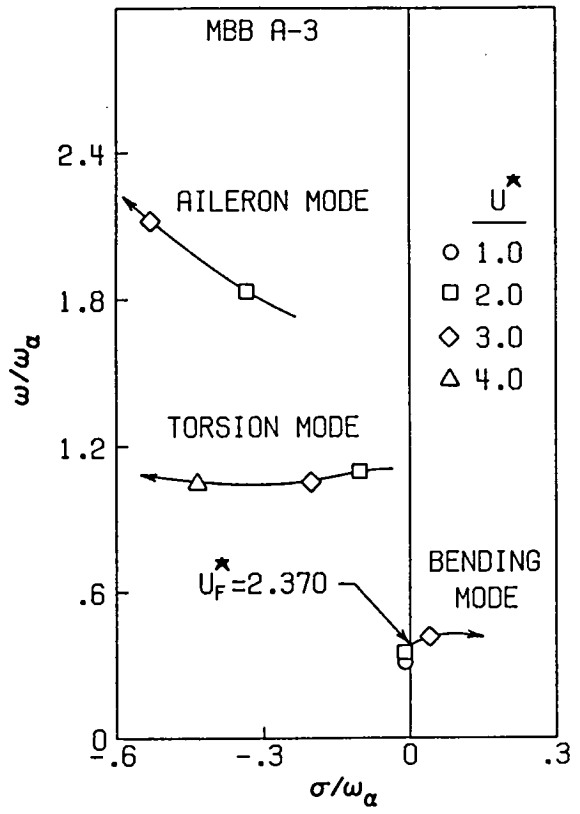

Fig. 3 MBB A-3 open-loop flight speed root-loci at M = 0.765 and c_ℓ = 0.58.

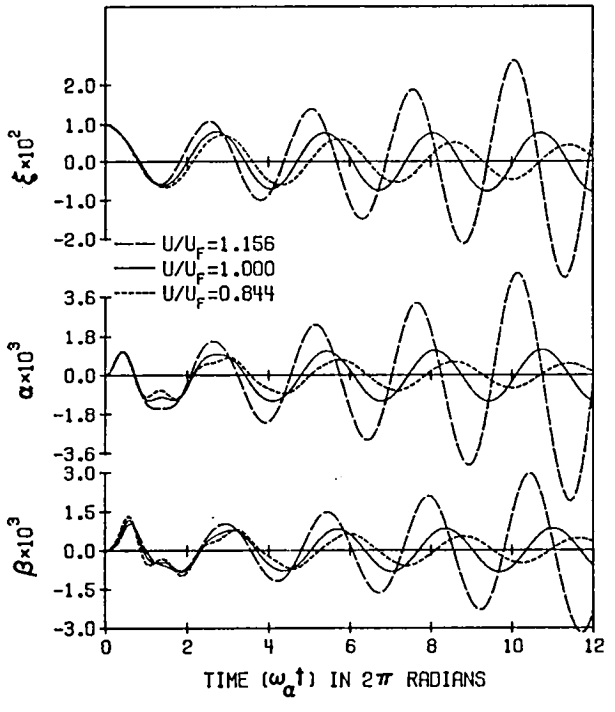

Fig. 4 Effect of flight speed on MBB A-3 open-loop time-marching displacement responses at M = 0.765 and c_ℓ = 0.58.

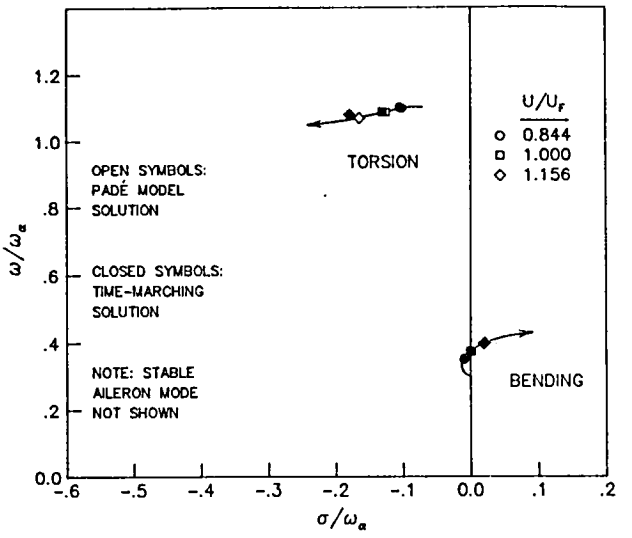

Fig. 5 MBB A-3 flight speed root-loci for bending and torsion modes at M = 0.765 and c_ℓ = 0.58.

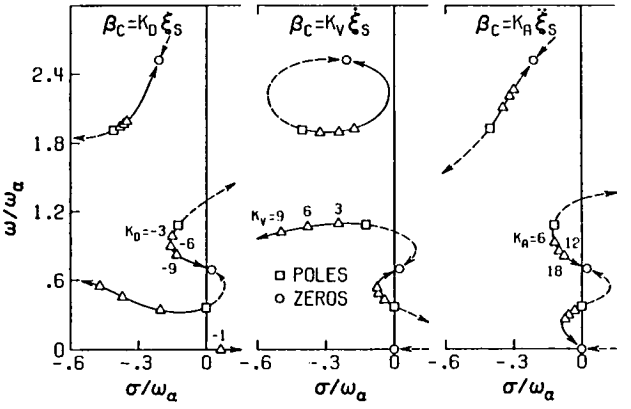

Fig. 6 MBB A-3 control gain root-loci at the open-loop flutter speed ($U^* = U_F^*$), M = 0.765 and c_ℓ = 0.58.

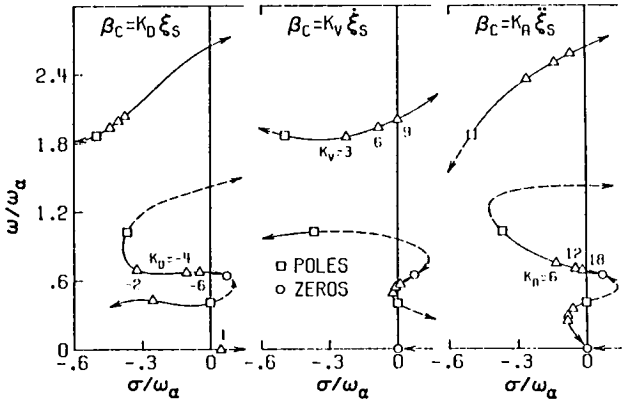

Fig. 7 Control gain root-loci at the open-loop flutter speed ($U^* = U_F^*$) computed using linear subsonic aerodynamic theory at M = 0.765.

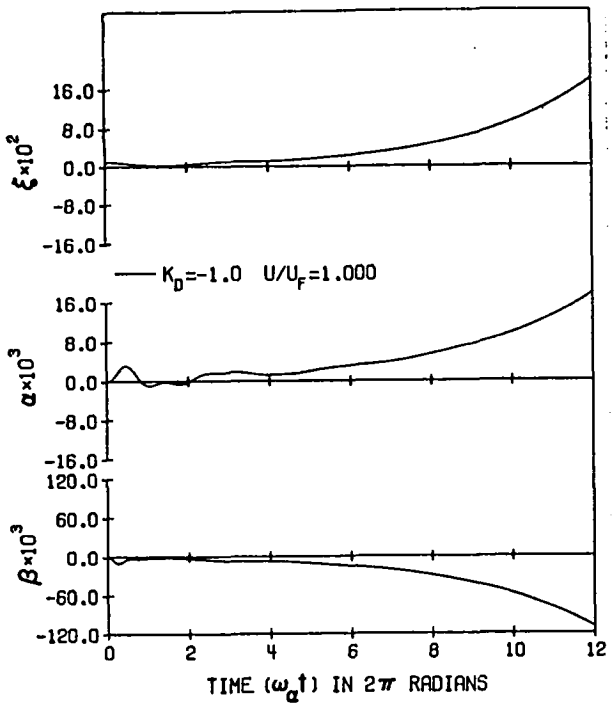

Fig. 8 Effect of displacement feedback on MBB A-3 time-marching displacement responses at the open-loop flutter speed U/U_F = 1.0, M = 0.765 and c_ℓ = 0.58.

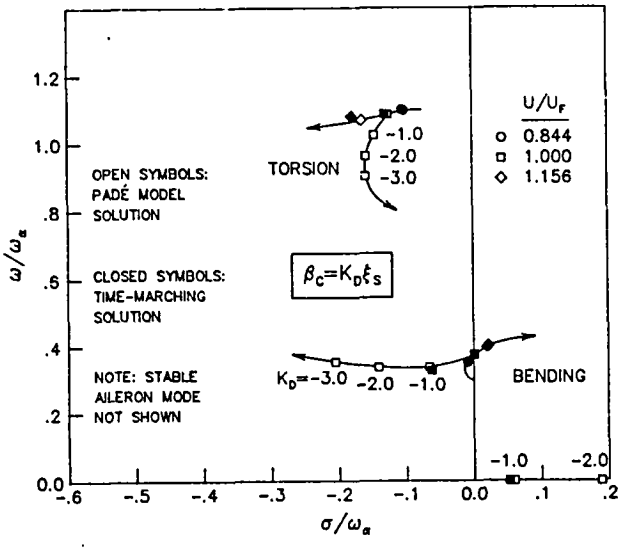

Fig. 9 Effect of displacement feedback on MBB A-3 bending and torsion modes at the open-loop flutter speed U/U_F = 1.0, M = 0.765, and c_ℓ = 0.58.

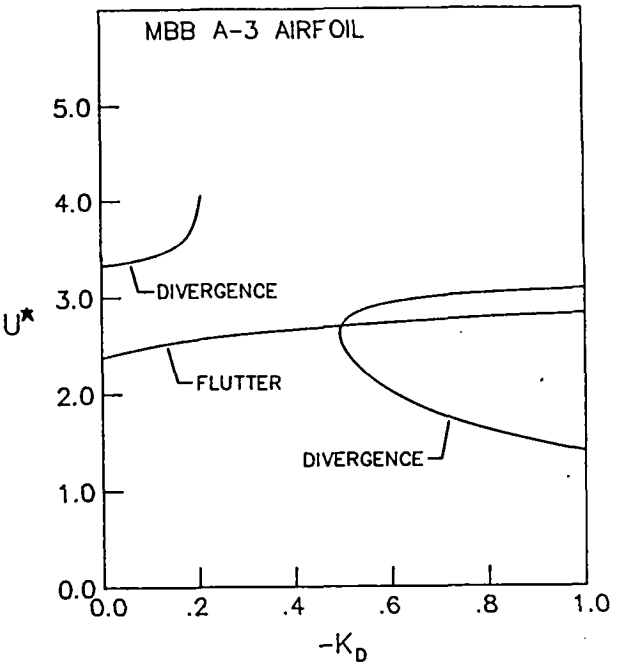

Fig. 10 Effect of negative displacement feedback on MBB A-3 flutter and divergence speeds at M = 0.765 and c_ℓ = 0.58.

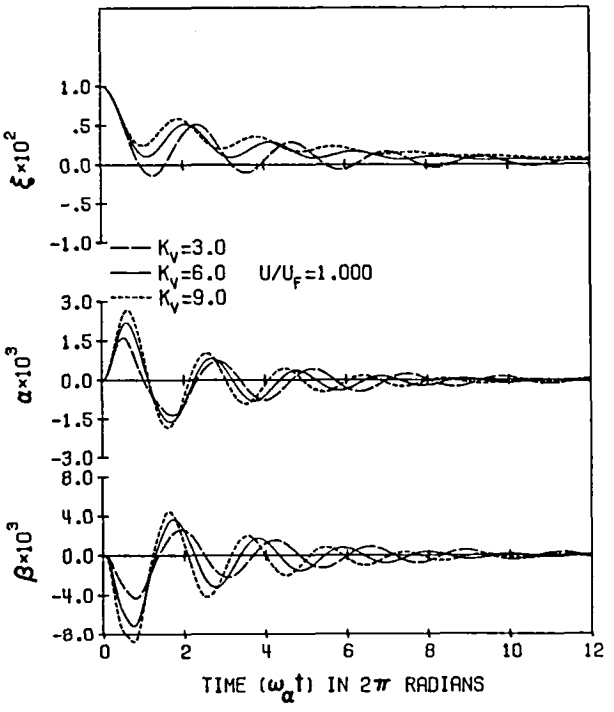

Fig. 11 Effect of velocity feedback on MBB A-3 time-marching displacement responses at the open-loop flutter speed U/U_F = 1.0, M = 0.765 and c_ℓ = 0.58.

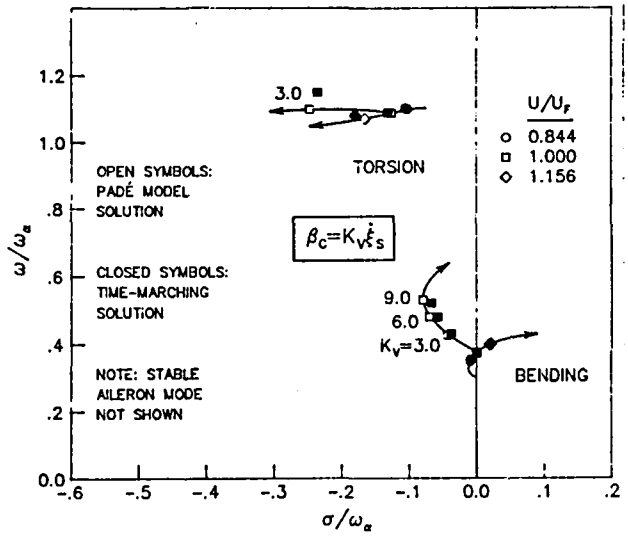

Fig. 12 Effect of velocity feedback on MBB A-3 bending and torsion modes at the open-loop flutter speed $U/U_F = 1.0$, $M = 0.765$ and $c_\ell = 0.58$.

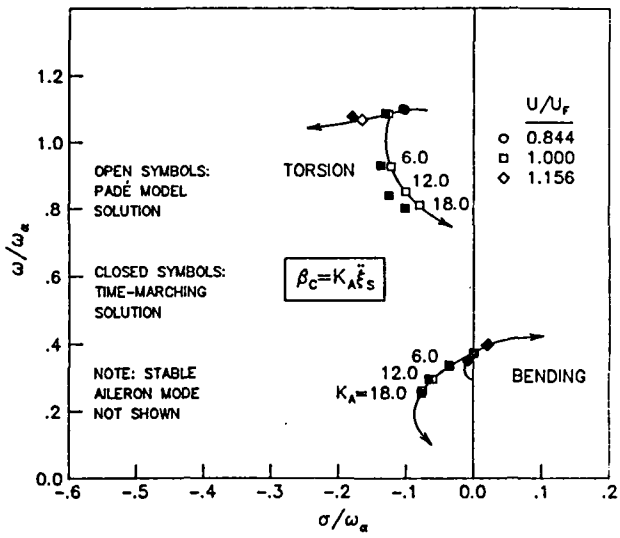

Fig. 14 Effect of acceleration feedback on MBB A-3 bending and torsion modes at the open-loop flutter speed $U/U_F = 1.0$, $M = 0.765$ and $c_\ell = 0.58$.

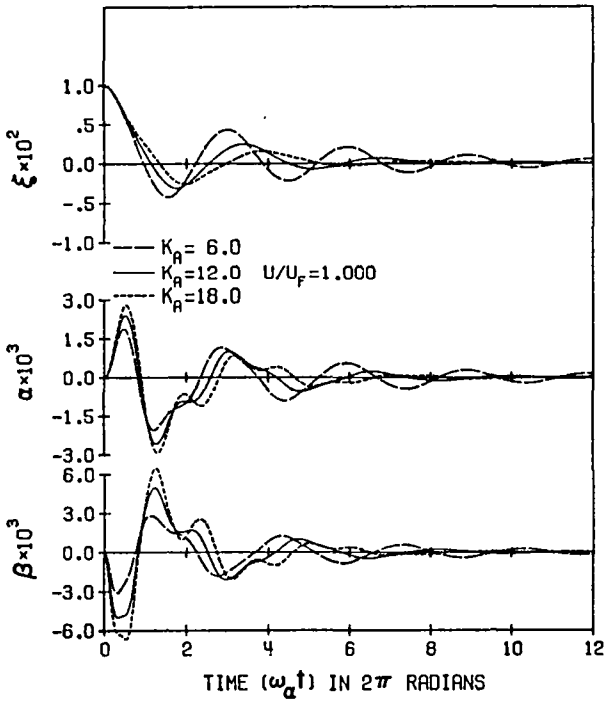

Fig. 13 Effect of acceleration feedback on MBB A-3 time-marching displacement responses at the open-loop flutter speed $U/U_F = 1.0$, $M = 0.765$ and $c_\ell = 0.58$.

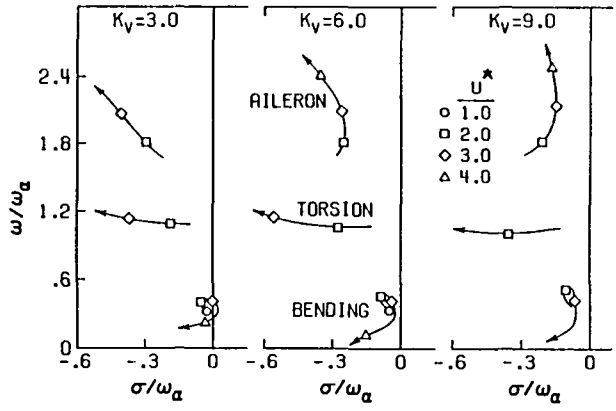

Fig. 15 MBB A-3 velocity feedback, flight speed root-loci at $M = 0.765$ and $c_\ell = 0.58$.

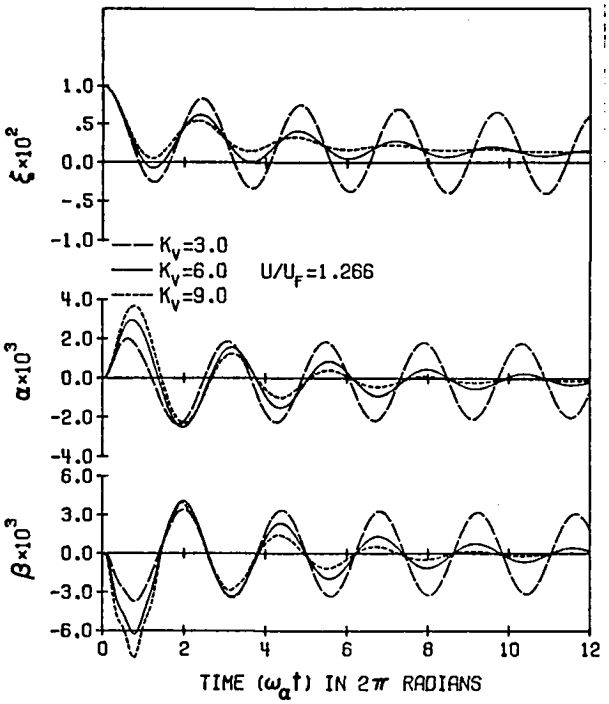

Fig. 16 Effect of velocity feedback on MBB A-3 time-marching displacement responses at U/U_F = 1.266, M = 0.765 and c_ℓ = 0.58.

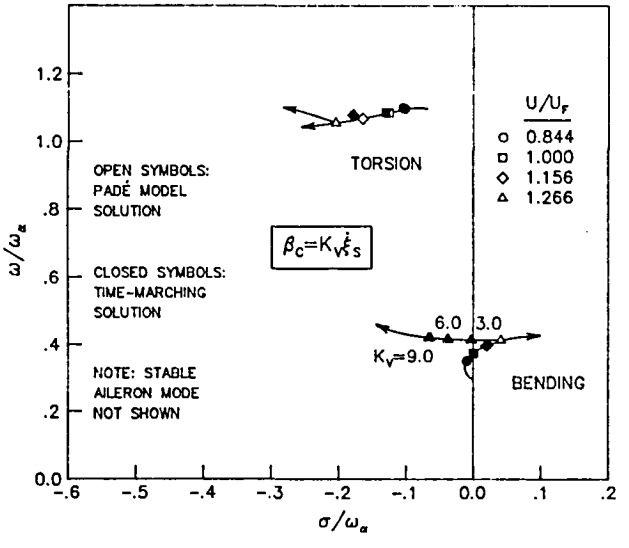

Fig. 17 Effect of velocity feedback on MBB A-3 bending and torsion modes at U/U_F = 1.266, M = 0.765 and c_ℓ = 0.58.

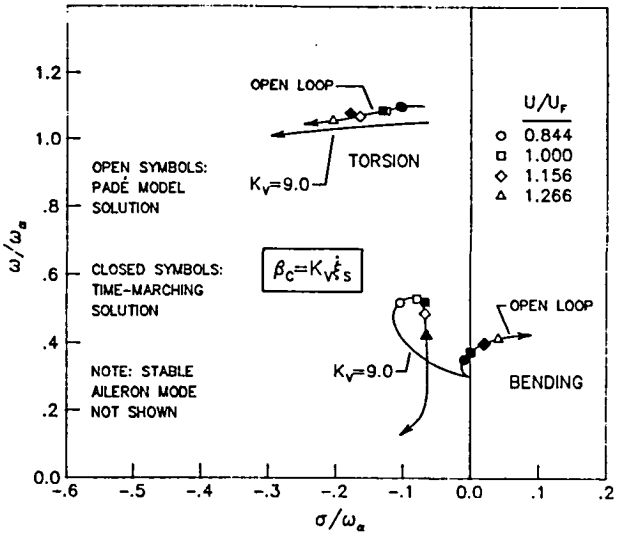

Fig. 18 MBB A-3 open and closed (K_V = 9.0) loop flight speed root-loci for bending and torsion modes at M = 0.765 and c_ℓ = 0.58.

1. Report No.	2. Government Accession No.	3. Recipient's Catalog No.
NASA TM-85770		

4. Title and Subtitle	5. Report Date
TRANSONIC CALCULATION OF AIRFOIL STABILITY AND RESPONSE WITH ACTIVE CONTROLS	March 1984
	6. Performing Organization Code: 505-33-43-09
7. Author(s): John T. Batina and T. Y. Yang	8. Performing Organization Report No.
9. Performing Organization Name and Address: NASA Langley Research Center, Hampton, VA 23665	10. Work Unit No.
	11. Contract or Grant No.
12. Sponsoring Agency Name and Address: National Aeronautics and Space Administration, Washington, DC 20546	13. Type of Report and Period Covered: Technical Memorandum
	14. Sponsoring Agency Code

15. Supplementary Notes

John T. Batina, NASA Langley Research Center, Hampton, Virginia
T. Y. Yang, Purdue University, West Lafayette, Indiana

16. Abstract

Transonic aeroelastic stability and response analyses are performed for the MBB A-3 supercritical airfoil. Three degrees of freedom are considered: plunge, pitch, and aileron pitch. The objective of this study is to gain insight into the control of airfoil stability and response in transonic flow. Stability analyses are performed using a Padé aeroelastic model based on the use of the LTRAN2-NLR transonic small-disturbance finite-difference computer code. Response analyses are performed by coupling the structural equations of motion to the unsteady aerodynamic forces of LTRAN2-NLR. The focus of the present effort is on transonic time-marching transient response solutions using modal identification to determine stability. Frequency and damping of these modes are directly compared in the complex s-plane with Padé model eigenvalues. Transonic stability and response characteristics of 2-D airfoils are discussed and comparisons are made. Application of the Padé aeroelastic model and time-marching analyses to flutter suppression using active controls is demonstrated.

17. Key Words (Suggested by Author(s))	18. Distribution Statement
Unsteady Aerodynamics Aeroelasticity Active Control Flutter	Unclassified - Unlimited Subject Category 02

19. Security Classif. (of this report)	20. Security Classif. (of this page)	21. No. of Pages	22. Price
Unclassified	Unclassified	12	A02

For sale by the National Technical Information Service, Springfield, Virginia 22161